




Three-dimensional visualization technique compared with magnetic resonance cholangiopancreatography for evaluation of anatomic variants of pediatric congenital choledochal cysts

Peng Wang^{1,2} · Yiming Gong¹ · Shijiao Lu² · Jie Chen^{1,2} 

Accepted: 29 December 2020 / Published online: 28 January 2021

© The Author(s), under exclusive licence to Springer-Verlag GmbH, DE part of Springer Nature 2021

Abstract

Objective The aim of this study was to compare the application of a three-dimensional (3D) visualization technique and magnetic resonance cholangiopancreatography (MRCP) for diagnosis of pediatric congenital choledochal cysts.

Methods Thin slices of coronal heavily T2-weighted pulse sequences of MRI pertaining to 35 patients were retrospectively used to reconstruct 3D models. Diagnoses and variants of the biliary system were evaluated based on the 3D models and MRCP imaging. The quality of delineation of the biliary duct system and the Todani classification were evaluated. Wilcoxon and Chi-squared tests were used for statistical analysis.

Results Two cases that were diagnosed as type II congenital choledochal cysts using the 3D model were diagnosed as type I using MRCP imaging. Significant differences were observed between the two modalities with respect to the delineation of the right anterior bile duct, right posterior bile duct, and left hepatic duct. The excellent and good rates obtained with the 3D model (65.7%) were much better than that obtained with MRCP (37.1%) imaging. Two cases with accessory hepatic ducts (5.7%), one case with an accessory pancreatic duct (2.8%), and two cases with biliary strictures at the hepatic hilum (5.7%) were detected using the 3D models. In contrast, only one case with an accessory hepatic duct and one case with a biliary stricture at the hepatic hilum were detected using MRCP.

Conclusion The 3D visualization technique facilitated more precise morphological evaluation of congenital choledochal cysts and provided comprehensive spatial anatomic information for diagnosis.

Keywords Heavily T2-weighted · MRCP · 3D visualization · Pediatric congenital choledochal cyst

Introduction

Pediatric congenital choledochal cyst (CC) is a common malformation of the biliary tract. The estimated incidence in Asian children is 1:1000 [1]. Several imaging modalities are used for diagnosis of CC such as ultrasonography, computed tomography (CT), magnetic resonance

cholangiopancreatography (MRCP), endoscopic retrograde cholangiopancreatography (ERCP), and intraoperative cholangiopancreatography (IOC) [2–6]. MRCP is the modality-of-choice for radiologic diagnosis owing to its noninvasive nature and lack of radiation exposure [7, 8]; however, MRCP images are obtained using the maximum intensity projection (MIP) technique, which is a two-dimensional imaging method. In addition, it may result in an inaccurate diagnosis due to overlapping variant anatomy, torsion, or adhesion of the ducts [9, 10]. Furthermore, MRCP imaging is prone to false-negative results when used without a source coronal or axial imaging evaluation. This limitation is even more pronounced in the hands of inexperienced radiologists or clinicians.

Three-dimensional (3D) visualization is a modern computer-aided surgical technique that converts CT or MRI data into a 3D model using procedural imaging operations. The rendered model can facilitate surgical planning by providing

Yiming Gong contributed equally to this work as co-first author.

✉ Jie Chen
jjechen1974@163.com

¹ Department of Pediatric Surgery, Xinhua Hospital, School of Medicine, Shanghai Jiao Tong University, No. 1665 of Kongjiang Road, Yangpu District, Shanghai 200092, China

² Department of Pediatric Surgery, Jiaying Maternity and Child Health Care Hospital, No. 2468 of Central East Road, Nanhu District, Jiaying 314000, China

in-depth delineation of the pathological anatomy [11–13]. MRCP imaging is based on the apparent grayscale contrast between static liquid and the surrounding tissues using slices obtained from heavily T2-weighted pulse sequences [8]. Theoretically, it is feasible to perform 3D visualization using the imaging threshold and segmentation. In the present study, we applied the 3D visualization technique to convert the slice source data for CCs into 3D models to provide an advanced evaluation of the anatomy of the biliary system.

Materials and methods

Clinical data

This study was approved by the Ethics Committee of the Xin Hua Hospital Affiliated to the Shanghai Jiao Tong University School of Medicine (approval number: XHEC-D-2020-113) and Ethics Committee of the Jiaxing Maternity and Child Health Care Hospital affiliated to the Jiaxing College (approval number: 2019-88). The authors reviewed the MRCP data of CCs diagnosed during the period 2013–2017. The exclusion criteria were: (1) history of previous biliary surgery; (2) low-quality imaging; and (3) lack of coronal source data. After applying these exclusion criteria, data pertaining to 35 patients were included in the study. The clinical data are shown in Table 1.

Equipment and the MRCP protocol

The MRCP protocol was performed using a 1.5T scanner with 8-channel body surface array coils and a respiratory trigger (UIH, uMR560; United Imaging Medical Technology, Inc., Shanghai, China). The MRCP protocol included the following routine sequences: (1) 3D T2-weighted fast spin-echo (FSE) with fat suppression in the coronal plane (repetition time [TR], 2000–3490 ms; echo time [TE], 700–900 ms; field of view [FOV], 250 × 250 mm; matrix,

256 × 256; and slice thickness, 1.0 mm with a 0.8 mm gap); and (2) single-shot FSE radial slices in the coronal plane (TR, 5764 ms; TE, 740 ms; FOV, 250–380 mm; matrix, 320 × 320; and slice thickness, 30–40 mm). The slices were acquired with the patient holding their breath (for older children) and during the shallower phase of respiration (in younger children). Gadolinium-based contrast medium and secretin were not administered. The post-processing imaging technique for MIP was applied for presentation.

3D visualization technique and equipment

The 3D visualization technique was performed using 3D software (MIMICS 20.0; Materialize, HQ, Leuven, Belgium). First, the source data were imported into the software and converted into a project file. Second, appropriate thresholding was applied for mask building. Third, region growing, morphologic operations, and imaging editing were combined for advanced image segmentation. Finally, the 3D visualization model was calculated from the mask.

The 3D visualization model and MRCP imaging evaluation

The 3D visualization model and MRCP images were acquired independently after the blinding of clinical information. The 3D visualization model and MRCP images were evaluated by a senior pediatric radiologist with 3 years of abdominal MRI experience and a senior pediatric surgeon with 3 years of biliary surgery experience. Any differences in interpretation were resolved by consensus. The Todani classification was used for diagnosis with both methods [14]. The Papanikolaou and Lim methods were used to evaluate the quality of delineation of biliary tract [15, 16], while the anatomical variations in the biliary system were assessed using the Couinaud and Komi classifications [17, 18]. Pancreato-biliary junction malformations (PBMs) were identified as a long common channel with a length > 15 mm. Anatomic variations, such as accessory pancreatic duct (APD), accessory hepatic duct (AHD), and biliary strictures (BSs) at the hepatic hilum, were investigated. BS was defined as a change in diameter between the dilated biliary duct on the liver side and the duct on the duodenal side.

Statistical analysis

Statistical analysis was performed using SPSS 18.0 software (IBM, Inc., Chicago, IL, USA). The two-sided Wilcoxon's test was used to compare bile duct evaluation and imaging quality. The variation rate was compared using the Chi-squared test. *P* values ≤ 0.05 were considered indicative of statistical significance.

Table 1 General clinical data

Variables	Data
Sex (<i>n</i>)	Boys: 8; girls: 27
Age	Mean age: 3.05 years; range: 2 months to 10 years
Todani classification	
Type I	31
Type II	0
Type III	0
Type IV	4
Type V	0

Results

Comparison of the results of Todani classification

The 3D visualization model distinctly delineated the morphology of cysts and the biliary system. Moreover, it provided in-depth delineation of the proximal and distal variations, the left and right segments of the ducts, and the portion of the bile duct. The results of the Todani classification are shown in Table 2. Few differences were observed in the diagnosis using the two methods. Two cases were diagnosed as type I congenital CCs with MRCP imaging and as type II using the 3D visualization model (Figs. 1, 2). There was no significant difference between the two imaging modalities in this respect ($\chi^2 = 1.034, P = 0.793$).

Comparison of imaging quality

There was no significant difference with respect to the image quality of the common bile duct (CBD) and third bile duct based on the Papanikolaou method ($P = 1.000$ and $P = 0.063$, respectively). Visualization of the right anterior (RA) bile, right posterior (RP) bile, and left (L) hepatic ducts in the 3D model was significantly better than that in MRCP images ($P = 0.000, P = 0.000$, and $P = 0.007$, respectively). According to the Lim method for evaluating image quality, the excellent and good rates with the 3D visualization model (65.7% [23/35]) were significantly higher than that with MRCP images (37.1% [13/35]; $\chi^2 = 5.719, P = 0.017$).

Table 2 Results of the Todani classification

	I	II	III	IV	V	Total
3D	29	2	0	4	0	35
MRCP	31	0	0	4	0	35

$\chi^2 = 1.034; P = 0.793$

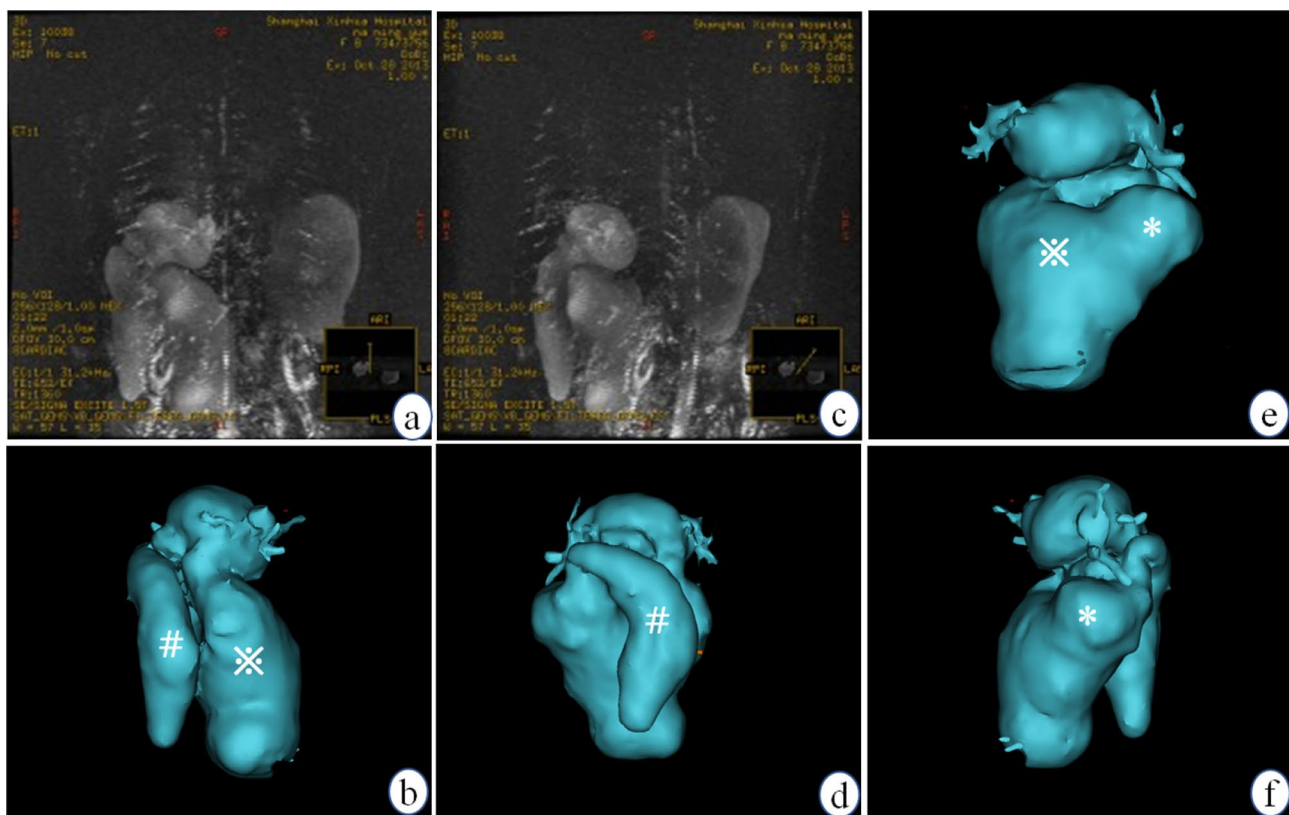


Fig. 1 Eight-year-old girl. She was diagnosed as a case of type I congenital CC with MRCP (a, c) and as type II CC with the 3D model (e, b, d, f). The 3D model clearly delineated the cyst morphology, its

relationship with adjacent structures, and the confluence of the neck of the gallbladder with the diverticulum of the CC (# indicates the gallbladder; ✕ indicates the CC; * indicates the diverticulum)

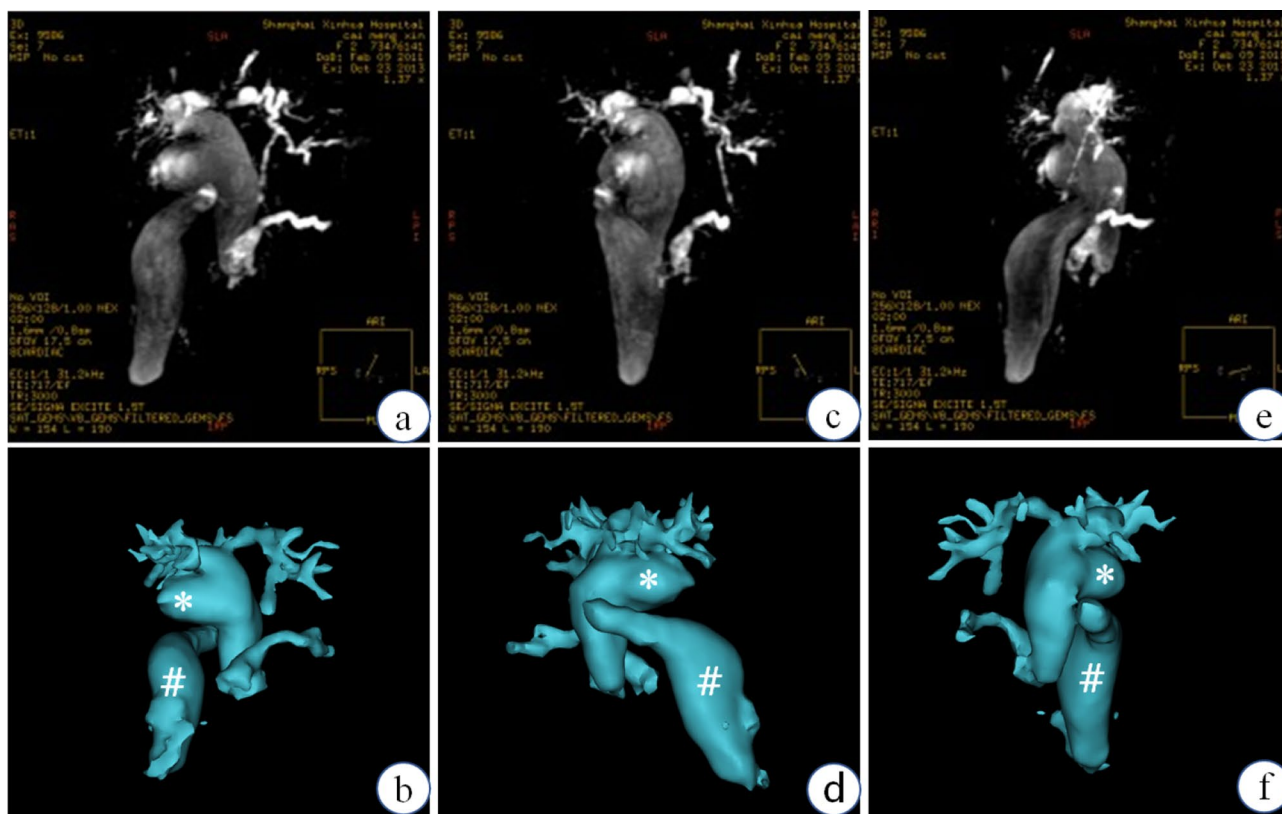


Fig. 2 Two-year-old girl. She was diagnosed as a case of type II congenital CC using the 3D model method (**b, d, f**) and as a suspected case of type II congenital CC using MRCP (**a, c, e**). Images presented a clear morphology, the level of location of the CC, and its relation-

ship with the adjacent structures, such as the gallbladder neck, common bile duct, and distal part of the duct (# indicates the gallbladder; * indicates a diverticulum)

Table 3 Proximal variations as assessed by the Couinaud classification

	A	B	C	D	Total
3D	29	3	1	2	17.1% (6/35)
MRCP	30	3	1	1	14.3% (5/35)

$$\chi^2 = 0.0235; P = 0.095$$

Comparison of the proximal region using the Couinaud classification

The proximal variations primarily included the bile and aberrant ducts. According to the Couinaud classification, 29, three, one, and two cases were classified as type A, B, C, and D choledochal cysts, respectively, in the 3D visualization model with a variation rate of 17.1% (6/35). In the MRCP group, 30, three, one, and one cases were classified as type A, B, C, and D choledochal cysts, respectively, with a variation rate of 14.3% (5/35). The results of the statistical comparisons are presented in Table 3. There

was no significant between-group difference in this respect ($\chi^2 = 0.235$, $P = 0.095$) (Figs. 3, 4).

Comparison of PBM with Komi classification

Based on the 3D visualization model, there were 4, 10, and 1 cases of type A, B, and C choledochal cysts, respectively. Based on the MRCP images, there were 3 and 9 cases of type A and B choledochal cysts, respectively. There was no significant between-group difference in this respect (Table 4). The 3D visualizations of the Komi classification are shown in Fig. 5.

Visualization rates of rare malformations

The visualization rates for APD, AHD, and BS are shown in Table 5. There was no significant difference between the two methods in this respect (APD, $\chi^2 = 1.014$, $P = 0.314$; AHD, $\chi^2 = 0.348$, $P = 0.555$; BS, $\chi^2 = 2.059$, $P = 0.151$). The 3D visualization model provided more clear delineation of the rare malformations compared with MRCP imaging (Fig. 6).

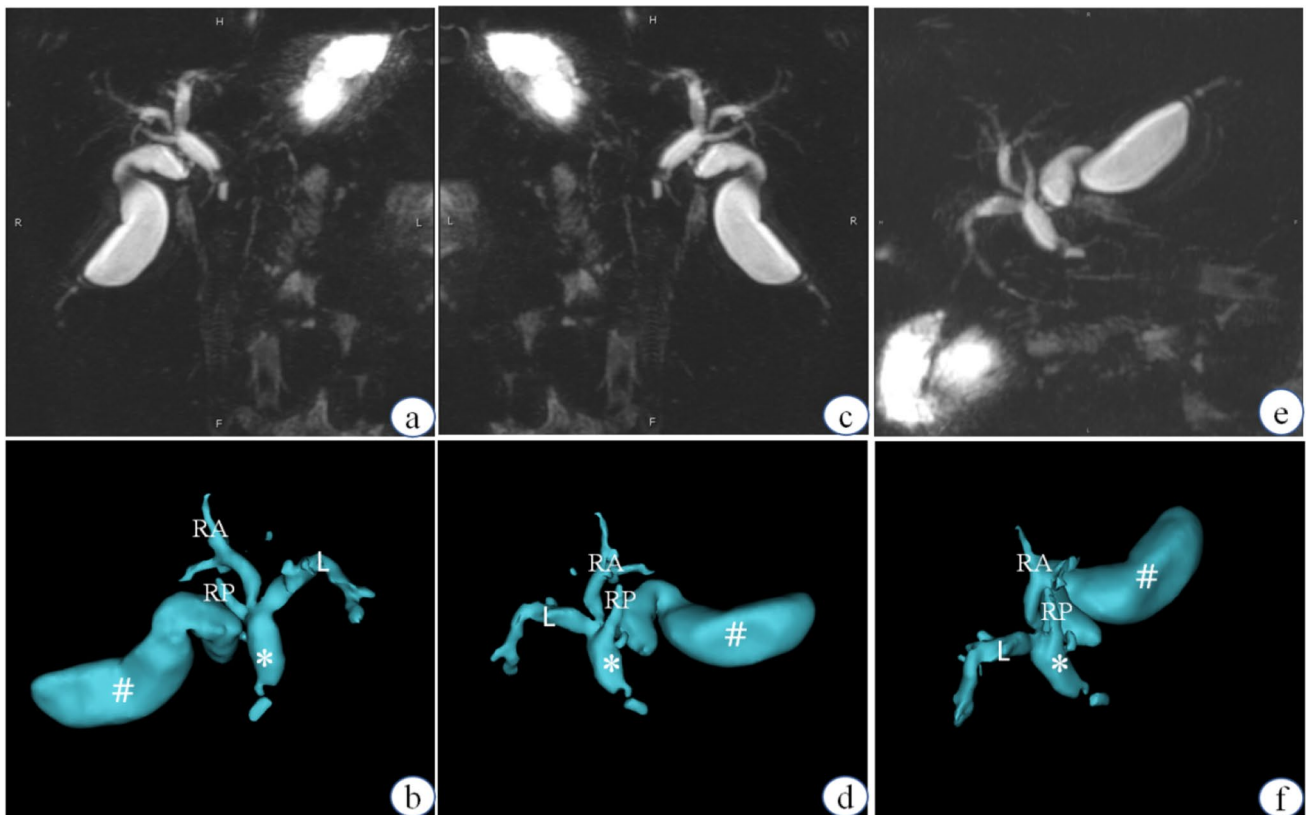


Fig. 3 Eighteen-month-old girl. **a, c, e** were classified as type B CC trifurcation based on the MRCP method; **b, d, f** were classified as RP confluence into the CC from the posterior side. *RA* right anterior

duct, *RP* right posterior duct, *L* left hepatic duct, *#* indicates the gallbladder, *** indicates CC

Discussion

The pathological anatomy of pediatric CCs is complex, considering the intra- and extra-biliary ducts, gallbladder, and each of the connecting regions. Lack of a definitive surgical plan is liable to increase the surgical risk and complications [18–21]. MRCP imaging is a noninvasive technique that uses a heavily T2 sequence pulse; it is the preferred method for delineating the anatomy of the biliary duct instead of CT [6, 22]. Many techniques, including gradient echo (GRE), fast spin echo (FSE), respiratory-trigger, 3D volume rendering, MIP, and many different coils, have been developed to improve the imaging quality. The MIP imaging quality is similar to that of ECRP and is widely used by clinicians due to the acquisition of isotropic source data from the 3D MRCP and the high signal-to-noise ratio [3]; however, the MIP technique has several limitations. The first limitation is the high rate of false-negative results because it is a post-processing imaging technique and liable to miss small stones or structures located outside the duct. Furthermore, MIP imaging is a two-dimensional technique and adhesions or torsion of the duct may lead to false-positive diagnosis of stricture. Thus, the acquisition of detailed information

of biliary structures is a key imperative to create a precise surgical plan and reduce post-surgical complications.

In the present study, most of the Todani classification results were similar between the 3D model and the MRCP imaging; however, some differences in the classification were observed with the MRCP imaging. One patient had a cyst protruding from the right middle aspect of the CBD and there was a confluence of the gallbladder duct with the distal part of the CBD; this patient was diagnosed as a type I CC with MRCP and as type II CC with the 3D model. Another case was diagnosed as type II CC with the 3D model which showed the protrusion of the structural cyst from the right posterior aspect of the CBD and confluence of the gallbladder duct with the proximal part of the cyst. Accordingly, the gallbladder was pushed and moved forward. These pathological changes were missed on MRCP imaging due to the overlapping structures leading to misdiagnosis.

The 3D visualization technique is a new method that converts the gray images into 3D models using interactive imaging processing. In the present study, the source data from the MRCP images were adequate for the reconstruction of 3D visualization models. The 3D model allowed detailed visualization of the morphology from each position; however,

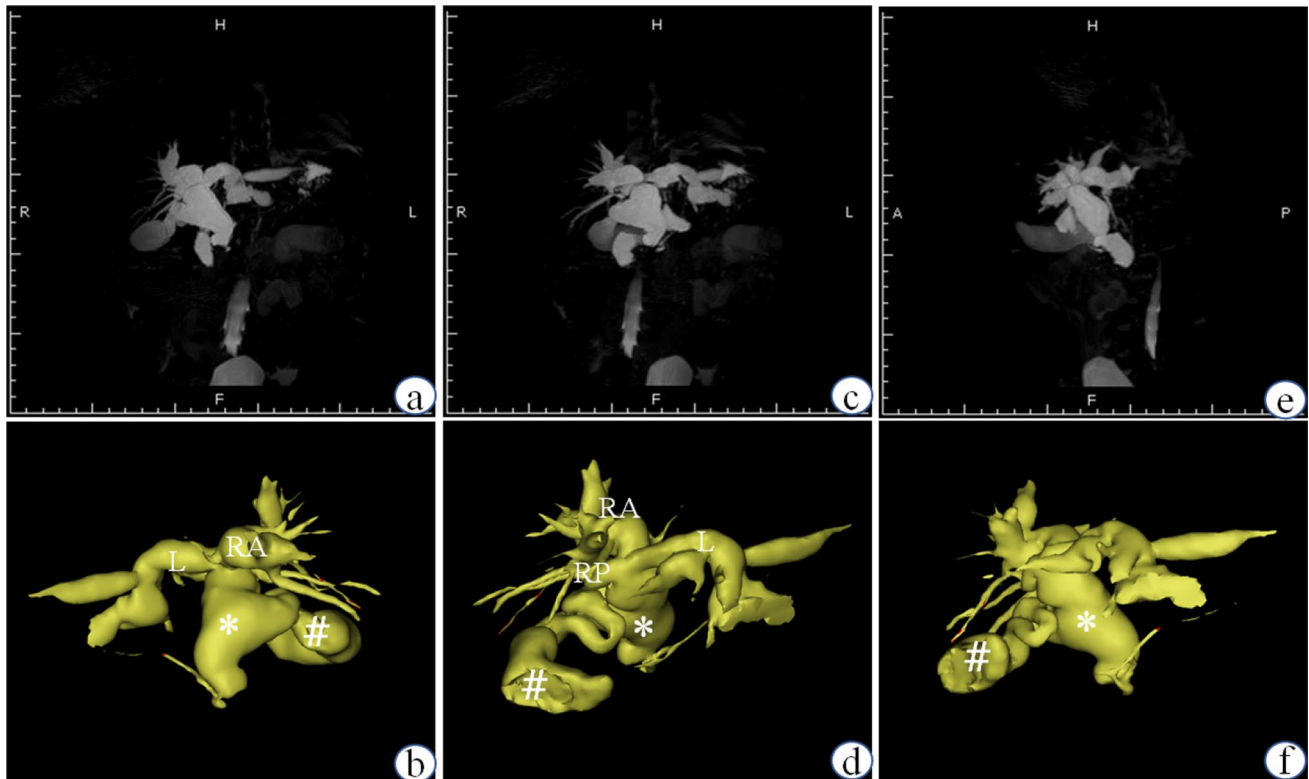


Fig. 4 Three-year-old girl. **a, c, e** Were diagnosed as type A CC by MRCP and as type B CC trifurcation by the 3D model in **b, d, f**. RA right anterior duct, RP right posterior duct, L left hepatic duct, # indicates the gallbladder, * indicates the CC

Table 4 Comparison of the distal region using the Komi classification

	A	B	C	Total
3D	4/35	10/35	1/35	42.8% (15/35)
MRCP	3/35	9/35	0/35	34.3% (12/35)

$$\chi^2 = 0.873; P = 0.646$$

this technique is based on post-processing of the source data. Therefore, it can miss some of the primary data resulting in distortion of the 3D model. In this study, the rate of excellent classification using the 3D model (62.8%) was considerably higher than that for MRCP imaging (37.1%) due to the intuitive presentation and detail of the 3D visualization model.

There was no discernible difference between the two methods with respect to the delineation of the CBD and third-level branches of ducts because of the high-quality source data and the similarities of the biliary system anatomy, which can result in correct segmentation and imaging editing; however, the 3D visualization model afforded better delineation of the RA bile duct, RP bile duct, and L hepatic duct as compared to MRCP images. The 3D model clearly showed the confluence of each duct while the overlapping structures and variations in the biliary duct obscured the confluence in MRCP images.

The biliary tree is divided into three parts (proximal part, the level of the cyst, and the distal part), keeping in mind the limitations of the descriptions in the Todani classification for the entire biliary duct pathology and exact variations. The proximal variations included variations of the left and right hepatic ducts, the gallbladder confluence, and the AHD. Lal [21] reviewed 117 MRCP imaging data sets of pediatric CCs. Of these, 17 cases (14.5%) exhibited proximal variations [21]. The variation rates for MRCP imaging and one of the 3D visualization models was 4.3% and 17.1%, respectively; however, the between-group difference in this respect was not statistically significant. Nevertheless, the 3D visualization models clearly showed the variations (especially in the hepatic duct and right biliary duct) as well as the confluence.

Moreover, hepatic BSs and the presence of AHD are essential considerations in the pre-surgical plan. Neglecting the BSs may lead to postoperative cholangitis, hepatolithiasis, or carcinogenesis [23, 24]. Saito et al. [4] reported BSs in MRCP images of 6 out of 117 cases of pediatric CC, which was in agreement with our results (2/35 [5.7%]). Using the 3D visualization model, we measured the stricture parameters and analyzed the relationship of the BS with the adjacent structures, providing a detailed reference for bile duct-plasty. Furthermore, two

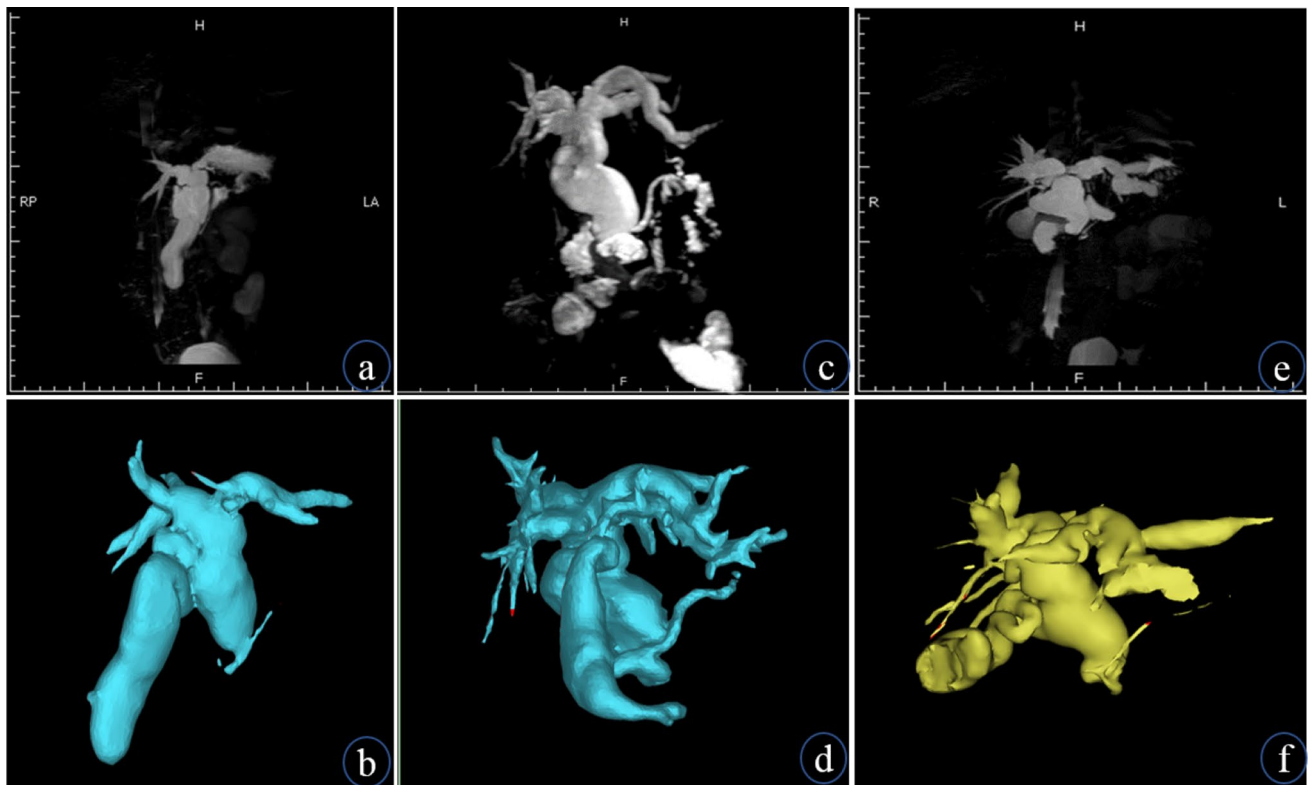


Fig. 5 The 3D model depiction of the Komi classification. **b** was classified as a type A CC using the 3D visualization model, but not with the corresponding MRCP images. **a, d** was identified as a type B CC using the 3D visualization model compared to the obscure result

demonstrated with MRCP imaging, which is presented in **c, f** was also diagnosed as a type C choledochal cyst (complicated), but this was not validated in the MRCP imaging results presented in **e**

Table 5 Visualization rates for rare malformations

	APD	AHD	BS
3D	1 (2.8%)	2 (5.7%)	2 (5.7%)
MRCP	0	1 (2.8%)	0

APD, $\chi^2=1.014, P=0.314$; AHD, $\chi^2=0.348, P=0.555$; BS, $s^2=2.059, P=0.151$

cases of ABDs were detected using the 3D visualization model. The results showed that the ABDs were similar to other studies, as indicated by IOC. In our study, AHD was missed in one case on MRCP imaging because the AHD was short and flowed into the CBD from the left side, which was covered by the cyst and confirmed with IOC.

The distal variation, known as PBM, also greatly influences the surgical protocol. Correct identification of the variation type can help avoid injury to the pancreatic duct. In the study by Saito et al. [4], 57% of 45 patients with CCs had concomitant PBM. In this study, the rate detected by the 3D visualization model (42.8%) was better than that detected with MRCP imaging (34.3%). The 3D

visualization model identified the type of PBM, the confluence, and the length of the pancreatic duct.

There were several limitations to this study. Although the 3D visualization technique reveals the morphology of the pathologic changes, 3D visualization utilizes serial image processing, which can influence the accuracy and the quality of the derived model without using the source data; however, high-quality source data and an experienced technologist can construct a high-quality model to make up for the loss of information. Thus, good communication with the radiologist is essential to provide instructions for scanning before the application of images in clinical practice.

Conclusion

The 3D visualization technique helped overcome the limitations of MRCP imaging by providing more in-depth information about the anatomy and structural variations. Therefore, 3D visualization represents a useful modality for the diagnosis of pediatric CCs and assessment of biliary variations.

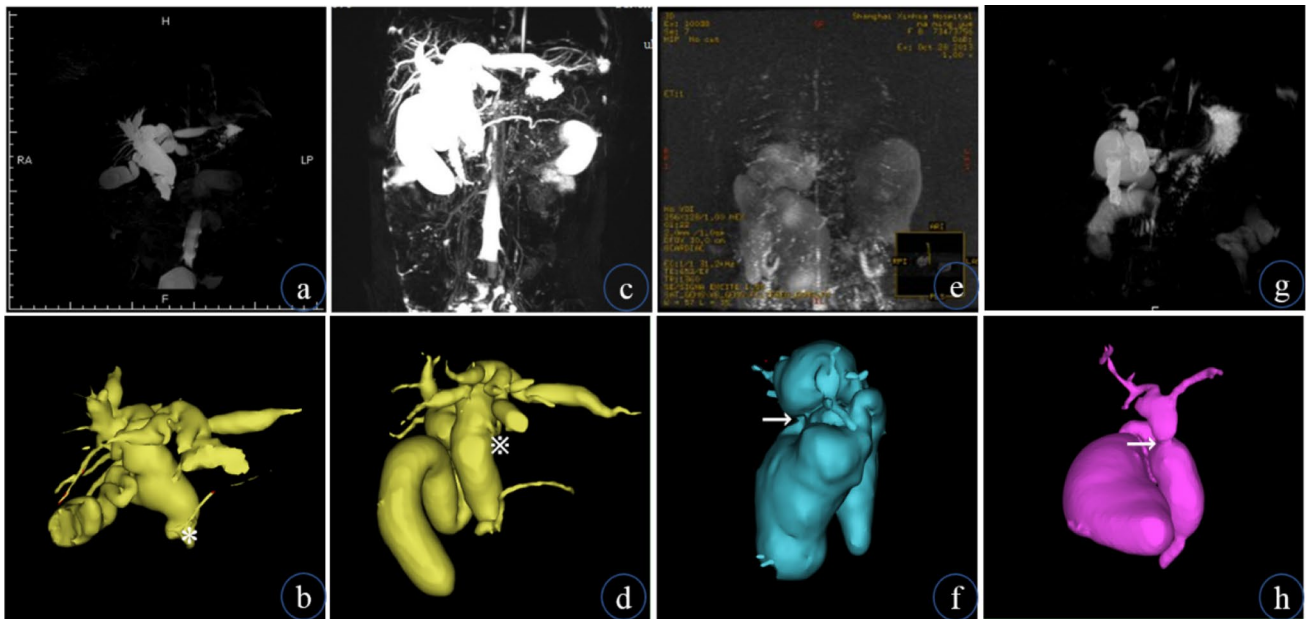


Fig. 6 Comparative delineation of APD, AHD, and BS with MRCP and the 3D model. **a, b** Show complicated APD (*). **c, d** show AHD (*). **e–h** Show BS (→). *APD* accessory pancreatic duct, *AHD* accessory hepatic duct, *BS* biliary stricture

Funding This study was funded by the Zhejiang Provincial Natural Science Foundation of China (No. LY20C110003), Science and Technology Bureau of Jiaxing City, and the Foundation of Xin Hua Hospital (Grant No. JZPI201708).

Compliance with ethical standards

Conflict of interest No financial or non-financial benefits have been received or will be received from any party related directly or indirectly to the subject of this article.

Ethical approval All procedures performed in studies involving human participants were in accordance with the ethical standards of the institutional and/or national research committee and complied with the 1964 Helsinki Declaration and its later amendments or comparable ethical standards. The study was approved by the Ethics Committee of the Xin Hua Hospital Affiliated to the Shanghai Jiao Tong University School of Medicine (approval number: XHEC-D-2020-113) and Ethics Committee of the Jiaxing Maternity and Child Health Care Hospital affiliated to the Jiaxing College (approval number: 2019-88).

References

- Soares KC, Kim Y, Solvate G, Maithel S, Bauer TW, Marques H, Sobral M, Knoblich M, Tran T, Aldrighetti L, Jabbour N, Poultsides GA, Gamblin TC, Pawlik TM (2015) Presentation and clinical outcomes of choledochal cysts in children and adults: a multi-institutional analysis. *JAMA Surg* 150(6):577–584. <https://doi.org/10.1001/jamasurg.2015.0226>
- Lam WW, Lam TP, Saing H, Chan FL, Chan KL (1999) MR cholangiography and CT cholangiography of pediatric patients with choledochal cysts. *AJR Am J Roentgenol* 173(2):401–405. <https://doi.org/10.2214/ajr.173.2.10430145>
- Sacher VY, Davis JS, Sleeman D, Casillas J (2013) Role of magnetic resonance cholangiopancreatography in diagnosing choledochal cysts: case series and review. *World J Radiol* 5(8):304–312. <https://doi.org/10.4329/wjr.v5.i8.304>
- Saito T, Hishiki T, Terui K, Sato Y, Mitsunaga T, Terui E, Nakata M, Takenouchi A, Matsuura G, Yahata E, Ohno S, Sato H, Yanagawa N, Masuda Y, Yoshida H (2011) Use of preoperative, 3-dimensional magnetic resonance cholangiopancreatography in pediatric choledochal cysts. *Surgery* 149(4):569–575. <https://doi.org/10.1016/j.surg.2010.11.004>
- Hiramatsu T, Itoh A, Kawashima H, Ohno E, Itoh Y, Sugimoto H, Sumi H, Funasaka K, Nakamura M, Miyahara R, Katano Y, Ishigami M, Ohmiya N, Kaneko K, Ando H, Goto H, Hirooka Y (2015) Usefulness and safety of endoscopic retrograde cholangiopancreatography in children with pancreaticobiliary maljunction. *J Pediatr Surg* 50(3):377–381. <https://doi.org/10.1016/j.jpedsurg.2014.08.024>
- Fumino S, Ono S, Kimura O, Deguchi E, Iwai N (2011) Diagnostic impact of computed tomography cholangiography and magnetic resonance cholangiopancreatography on pancreaticobiliary maljunction. *J Pediatr Surg* 46(7):1373–1378. <https://doi.org/10.1016/j.jpedsurg.2011.01.026>
- Kim M-J, Han SJ, Yoon CS, Kim JH, Oh J-T, Chung KS, Yoo HS (2002) Using MR cholangiopancreatography to reveal anomalous pancreaticobiliary ductal union in infants and children with choledochal cysts. *AJR Am J Roentgenol* 179(1):209–214. <https://doi.org/10.2214/ajr.179.1.1790209>
- Mortelé KJ, Ros PR (2001) Anatomic variants of the biliary tree: MR cholangiographic findings and clinical applications. *AJR Am J Roentgenol* 177(2):389–394. <https://doi.org/10.2214/ajr.177.2.1770389>
- Onder H, Ozdemir MS, Tekbaş G, Ekici F, Gümüş H, Bilici A (2013) 3-T MRI of the biliary tract variations. *Surg Radiol Anat* 35(2):161–167. <https://doi.org/10.1007/s00276-012-1021-0>
- Park DH, Kim MH, Lee SS, Lee SK, Kim KP, Han JM, Kim SY, Song MH, Seo DW, Kim AY, Kim TK, Min YI (2004) Accuracy of magnetic resonance cholangiopancreatography for locating

- hepatolithiasis and detecting accompanying biliary strictures. *Endoscopy* 36:987–992. <https://doi.org/10.1055/s-2004-825812>
11. Lamadé W, Glombitza G, Fischer L, Chiu P, Cárdenas CE Sr, Thorn M, Meinzer HP, Grenacher L, Bauer H, Lehnert T, Herfarth C (2000) The impact of 3-dimensional reconstructions on operation planning in liver surgery. *Arch Surg* 135(11):1256–1261. <https://doi.org/10.1001/archsurg.135.11.1256>
 12. Mise Y, Tani K, Aoki T, Sakamoto Y, Hasegawa K, Sugawara Y, Kokudo N (2013) Virtual liver resection: computer-assisted operation planning using a three-dimensional liver representation. *J Hepatobiliary Pancreat Sci* 20(2):157–164. <https://doi.org/10.1007/s00534-012-0574-y>
 13. Ringe KI, Hartung D, von Falck C, Wacker F, Raatschen HJ (2014) 3D-MRCP for evaluation of intra- and extrahepatic bile ducts: comparison of different acquisition and reconstruction planes. *BMC Med Imaging* 14:16. <https://doi.org/10.1186/1471-2342-14-16>
 14. Todani T, Watanabe Y, Narusue M, Tabuchi K, Okajima K (1977) Congenital bile duct cysts: classification, operative procedures, and review of thirty-seven cases including cancer arising from choledochal cyst. *Am J Surg* 134(2):263–269. [https://doi.org/10.1016/0002-9610\(77\)90359-2](https://doi.org/10.1016/0002-9610(77)90359-2)
 15. Papanikolaou N, Karantanis AH, Heracleous E, Costa JC, Gourtsoyiannis N (1999) Magnetic resonance cholangiopancreatography: comparison between respiratory-triggered turbo spin echo and breath hold single-shot turbo spin echo sequences. *Magn Reson Imaging* 17(9):1255–1260. [https://doi.org/10.1016/s0730-725x\(99\)00074-0](https://doi.org/10.1016/s0730-725x(99)00074-0)
 16. Lim JS, Kim MJ, Myoung S, Park MS, Choi JY, Choi JS, Kim SI (2008) MR cholangiography for evaluation of hilar branching anatomy in transplantation of the right hepatic lobe from a living donor. *AJR Am J Roentgenol* 191(2):537–545. <https://doi.org/10.2214/AJR.07.3162>
 17. Couinaud C (1957) *Le foie: etudes anatomies et chirurgicales*. Masson & Cie, Paris, pp 530–532
 18. Komi N, Takehara H, Kunitomo K, Miyoshi Y, Yagi T (1992) Does the type of anomalous arrangement of pancreaticobiliary ducts influence the surgery and prognosis of choledochal cyst? *J Pediatr Surg* 27(6):728–731. [https://doi.org/10.1016/s0022-3468\(05\)80102-2](https://doi.org/10.1016/s0022-3468(05)80102-2)
 19. Chan KW, Lee KH, Tsui SY, Mou JW, Tam YH (2016) Laparoscopic management of antenatally detected choledochal cyst: a 10-year review. *Surg Endosc* 30(12):5494–5499. <https://doi.org/10.1007/s00464-016-4912-z>
 20. Lal R, Behari A, Hari RH, Sikora SS, Yachha SK, Kapoor VK (2013) Variations in biliary ductal and hepatic vascular anatomy and their relevance to the surgical management of choledochal cysts. *Pediatr Surg Int* 29(8):777–786. <https://doi.org/10.1007/s00383-013-3333-5>
 21. Joshi A, Rajpal K, Kakadiya K, Bansal A (2014) Role of CT and MRCP in evaluation of biliary tract obstruction. *Curr Radiol Rep* 2:72. <https://doi.org/10.1007/s40134-014-0072-x>
 22. Saito T, Terui K, Mitsunaga T, Nakata M, Yoshida H (2016) Significance of imaging modalities for preoperative evaluation of the pancreaticobiliary system in surgery for pediatric choledochal cyst. *J Hepatobiliary Pancreat Sci* 23:347–352. <https://doi.org/10.1002/jhbp.347>
 23. Ando H, Ito T, Kaneko K, Seo T, Ito F (1996) Intrahepatic bile duct stenosis causing intrahepatic calculi formation following excision of a choledochalcyst. *J Am Coll Surg* 183(1):56–60
 24. Uno K, Tsuchida Y, Kawarasaki H, Ohmiya H, Honna T (1996) Development of intrahepatic cholelithiasis long after primary excision of choledochal cysts. *J Am Coll Surg* 183(6):583–8

Publisher's Note Springer Nature remains neutral with regard to jurisdictional claims in published maps and institutional affiliations.